PCCP

PAPER

View Article Online
View Journal | View Issue

Cite this: *Phys. Chem. Chem. Phys.*, 2021, **23**, 5797

Spin-forbidden heavy-atom tunneling in the ring-closure of triplet cyclopentane-1,3-diyl†

Luís P. Viegas, * Cláudio M. Nunes and Rui Fausto

Received 7th January 2021,
Accepted 15th February 2021

DOI: 10.1039/d1cp00076d

rsc.li/pccp

In 1975, Buchwalter and Closs reported one of the first examples of heavy-atom quantum mechanical tunneling (QMT) by studying the ring closure of triplet cyclopentane-1,3-diyl to singlet bicyclo[2.1.0]pentane in cryogenic glasses. Since then, no clear theoretical evidence has been provided to elucidate how the intersystem crossing (ISC) and QMT are related in the reaction mechanism. In this work, we unequivocally show that at cryogenic temperatures, the ISC occurs solely in the quantum tunneling regime, with weak coupling non-adiabatic transition state theory rate constants predicting a spontaneous reaction in fair agreement with experimental observations. Despite its limitations, such an approach can be used to help unlock a comprehensive understanding of a variety of spin-forbidden chemical reactions in the low temperature regime.

1 Introduction

Quantum mechanical tunneling (QMT) has been a discussion topic in the scientific literature since the early history of quantum mechanics,[1] with its relevance to chemistry initially highlighted by Bell.[2,3] In his theoretical work, Bell concluded that a treatment including QMT "is necessary for any reaction involving the motion of a hydrogen atom or a proton" because of its low mass. Interestingly, QMT in chemistry is not limited to hydrogen atoms (H-atom tunneling), but it can also be directly observed in reactions involving the motion of heavier atoms (heavy-atom tunneling) such as carbon,[4–13] nitrogen[14,15] and even oxygen.[16] Such observations demonstrate the need to include QMT as a fundamental aspect in the understanding of chemical reactivity,[17] particularly of organic reactions.[18–24]

As far as the total electronic spin is concerned, QMT (H- or heavy-atom) can happen in two different contexts: when tunneling takes place in the same potential energy surface (PES), thus without any change in the total electronic spin (spin-allowed process) or when tunneling involves PESs of different total electronic spins[25] (spin-forbidden process). In the former scenario, a hypothetical occurrence of ISC is separate from the spin-allowed tunneling process, as reported in a previous work.[26] However, for the latter scenario, tunneling is responsible for the ISC itself. To the best of our knowledge, there are only two established cases[14,16] (Scheme 1) of direct experimental observation of spin-forbidden heavy-atom QMT, where the transformation from reactants to products is followed spectroscopically, both concerning reactions where the spin character of the electronic wavefunction changes once from reactants to products. One is the rearrangement of triplet trifluoroacetyl nitrene into the corresponding singlet isocyanate (Scheme 1a) in cryogenic matrices at 2.8 to 23 K reported by Abe, Zheng and coworkers.[14] The other is the cyclization of triplet *syn*-2-formyl-3-fluorophenylnitrene to singlet 4-fluoro-2,1-benzisoxazole (Scheme 1b) in argon matrices at 10 to 20 K reported by us.[16] Additionally, two[28,29] of the first proposed examples of heavy-atom QMT are also thought to occur through a spin-forbidden tunneling process. These concern triplet 1,3-diradicals that undergo C–C bond formation to form a singlet product as shown in Scheme 2. However, as stated by Borden[30] not long ago and despite very recent efforts,[31] the details concerning the ISC of the reactions shown in Scheme 2 are still unclear: does the tunneling take place in the triplet PES where it can then undergo ISC to the singlet, or is the tunneling responsible for the ISC? The objective

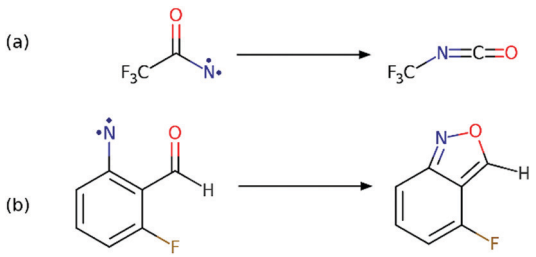

Scheme 1 Recent cases of spin-forbidden heavy-atom tunneling from a triplet ground-state reactant to a singlet product directly observed at cryogenic temperatures.[14,16] Structures displayed with MarvinSketch.[27]

University of Coimbra, CQC, Department of Chemistry, 3004-535 Coimbra, Portugal. E-mail: lpviegas@ci.uc.pt

† Electronic supplementary information (ESI) available: Cartesian coordinates for the stationary points of panel (a) in Fig. 1 and 2. Technical details of the electronic structure and rate constant calculations, with data collected in Tables S1–S4. See DOI: 10.1039/d1cp00076d

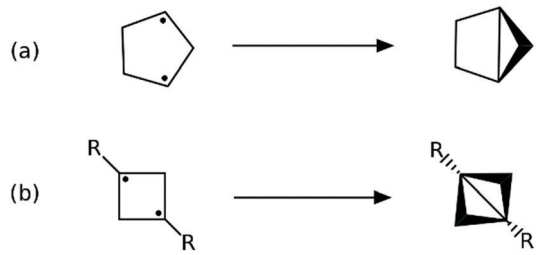

Scheme 2 Ring closure of (a) triplet cyclopentane-1,3-diyl to singlet bicyclo[2.1.0]pentane[28] and (b) triplet cyclobutane-1,3-diyl to singlet bicyclo[1.1.0]butane,[29] R = CH_3, CH_2CH_3. Structures displayed with MarvinSketch.[27]

of this work is to provide a definite clarification of the 45-year-old problem regarding the reaction mechanism of Closs's diradical (Scheme 2a) by computing the respective singlet and triplet PESs and then calculating the gas-phase rate constants for the consumption of the triplet diradical by explicitly taking into account the non-adiabatic nature of this spin-forbidden process.

2 Theory and computational methods

2.1 Potential energy surfaces

The singlet and triplet PESs for the reaction of Closs's diradical (Scheme 2a) are expected to display various degrees of multi-reference character,[32] requiring the use of multireference methods.[32–34] For cost-effective purposes we opted for the CASSCF(10,10)/cc-pV*T*Z level of theory,[35–39] which slightly improves the level of computation used on the thorough work performed by Carpenter.[34] The main objective of these calculations, which were all performed with GAMESS,[40] was to find minimum energy paths that included the cyclopentane-1,3-diyl reactant (triplet state) and the bicyclo[2.1.0]pentane product (singlet state). For this, we performed a series of saddle-point optimizations which were then followed by intrinsic reaction coordinate (IRC) runs and the respective minimization at the end points. Only two curves, one triplet and one singlet, fulfilled our requirements. The details of these curves are shown in Section 3. Enantiomeric pairings were numerically confirmed with a superimposing algorithm which is capable of evaluating geometrical similarity and has been extended to include enantiomer assignment.[41] At each stationary point, saddle-point or minimum, dynamical correlation (dc) was included with multiconfiguration quasi-degenerate perturbation theory (MC-QDPT)[42,43] at the MC-QDPT(10,10)/cc-pV*T*Z level. For the stationary points of panel (a), imaginary frequencies of saddle-points and total MC-QDPT electronic energies are collected in Table S1 of the ESI.†

2.2 Minimum energy crossing points

The importance of obtaining the minimum energy crossing point (MECP) in the context of spin-forbidden reactions is well documented.[25,44–47] The search for the MECP between the triplet and the singlet PESs was performed with the algorithm[48] available in GAMESS. The MECP is not a minimum in the full $3N - 6$ dimensions of either PESs, but rather a minimum on the crossing seam surface, which is a subspace of $3N - 7$ dimensions of those full PESs. Because of this reduced dimensionality, it is not possible to perform a typical frequency analysis at the end of an MECP search in GAMESS. This leads to two problems: (1) the zero-point energy (ZPE) correction for the MECP is not readily available and (2) the true nature of the stationary point on the crossing seam (minimum or saddle-point of any order) remains undetermined.[49] To overcome this problem, we can calculate a new effective Hessian matrix,[44,49] H_{eff}, which depends on the gradients of the two PESs at the MECP, $\mathbf{G_1}$ and $\mathbf{G_2}$, and also on the Hessians ($\mathbf{H_1}$ and $\mathbf{H_2}$) of this sloped intersection ($\mathbf{G_1}\cdot\mathbf{G_2} > 0$) between the two crossing PESs:

$$\mathbf{H}_{\text{eff}} = \frac{|\mathbf{G}_1|\mathbf{H}_2 - |\mathbf{G}_2|\mathbf{H}_1}{|\mathbf{G}_1 - \mathbf{G}_2|} \quad (1)$$

To perform vibrational analysis on the seam at the MECP, the reaction coordinate (which is orthogonal to the crossing seam) must be projected out[50] along with the three rotational and three translational degrees of freedom. After the projection, $\mathbf{H}_{\text{eff}}$ can be diagonalized to yield the $3N - 7$ vibrational frequencies corresponding to nuclear displacements on the seam surface. These can then be used to address points (1) and (2) above. To perform these steps, $\mathbf{H_1}$ and $\mathbf{H_2}$ were determined with Hessian calculations in GAMESS at the CASSCF(10,10)/cc-pV*T*Z level. Then we used gamread[16] to extract the geometry, $\mathbf{G_1}$, $\mathbf{G_2}$, $\mathbf{H_1}$ and $\mathbf{H_2}$ from the GAMESS outputs and datafiles and write them in the appropriate format to be read and used by the GLOWfreq[51] code. GLOWfreq performs the vibrational analysis of the MECP, yielding not only the respective vibrational frequencies and the ZPE, but also other necessary data to use in the rate constant calculations, which we will mention below.

2.3 Spin–orbit coupling

Spin–orbit coupling (SOC) is a relativistic effect with paramount importance[52,53] in the understanding of intersystem crossing (ISC) and its associated rate constants, since it is responsible for the mixing of electronic wavefunctions of different spin multiplicities and for determining the extent to which a specific spin-forbidden transition is actually allowed.[54] Our SOC calculations were based on variational configuration interaction wavefunctions (SO-CI method in GAMESS). Here, the SOC matrix elements between the singlet and the triplet states were evaluated by preparing a model Hamiltonian[52,53] containing the full Breit–Pauli spin–orbit operator in which the variational CI wavefunctions (CASCI basis[55]) were expanded in the reference CASSCF(10,10) wavefunction. This model Hamiltonian was then used[56] to calculate H_{SO}, the SOC constant.

2.4 Rate constant calculations

The ISC canonical temperature-dependent rate constant calculated through non-adiabatic transition state theory (NA-TST)[44,57–62] can be approximated[56,63] by using the properties of the Laplace

transform[64] and expressed as

$$k_{ISC}(T) = \frac{Q_{MECP}(T)}{hQ_R(T)} \int_0^\infty P_{trans}(\varepsilon_\perp) \exp(-\beta\varepsilon_\perp) d\varepsilon_\perp \quad (2)$$

where Q_{MECP} and Q_R are the partition functions at the MECP and reactant, respectively, $\beta = 1/k_BT$, P_{trans} is the probability of transition between two states at the MECP and $\varepsilon_\perp$ is the component of the internal energy accumulated in the reaction coordinate.

The probability of transition between two adiabatic (mixed-spin) PESs can be calculated with the Landau–Zener (LZ) formula[65–67]

$$p^{LZ}(\varepsilon_\perp) = \exp\left(-\frac{2\pi {H_{SO}}^2}{\hbar|\Delta\mathbf{G}|}\sqrt{\frac{\mu_\perp}{2(\varepsilon_\perp - E_{MECP})}}\right) \quad (3)$$

where $\mu_\perp$ is the reduced mass of the mode orthogonal to the crossing seam surface, E_{MECP} is the energy (total electronic energy plus ZPE) of the MECP relative to the minimum of the (triplet) spin-diabatic state where the reaction initiates (reactant R, in this case ^{3}**2**) defined as

$$E_{MECP} = E^{total}_{MECP} + E^{ZPE}_{MECP} - (E^{total}_R + E^{ZPE}_R) \quad (4)$$

H_{SO} is the SOC constant and $|\Delta\mathbf{G}|$ is the norm of the difference of the gradients on the two surfaces at the MECP, $|\Delta\mathbf{G}| = |\mathbf{G_1} - \mathbf{G_2}|$, which is orthogonal to the seam at the MECP. Here we are interested in calculating the probability of transition between the triplet and the singlet, *i.e.*, the two spin-diabatic PESs, which is then $1 - p^{LZ}$ and is often written considering the double passage version of the spin-diabatic LZ formula, introduced to describe unimolecular decomposition,[57] given by $P^{LZ}_{trans}(\varepsilon_\perp) = 1 - (p^{LZ})^2$. Note that in eqn (3), $p^{LZ}(\varepsilon_\perp)$ is defined only when the $\varepsilon_\perp$ internal energy is above the MECP ($\varepsilon_\perp > E_{MECP}$), failing at energies in the vicinity of E_{MECP} and neglecting transitions between PESs caused by quantum tunneling for energies below E_{MECP}. This means that the LZ formula does not consider the fact that the system does not need to reach the crossing region to hop from one spin-diabatic PES to the other, but may instead tunnel across. Naturally, such energy regimes can be of extreme importance when performing studies at cryogenic temperatures, since a thermal over-the-barrier process will most likely be ruled out in the vast majority of cases.

The quantum effects mentioned above can be accounted for in the more robust double passage weak coupling (WC) probability expression[57,68,69]

$$P^{WC}_{trans}(\varepsilon_\perp) = 4\pi^2 {H_{SO}}^2 \left(\frac{2\mu_\perp}{\hbar^2 \bar{G}|\Delta\mathbf{G}|}\right)^{2/3} \mathrm{Ai}^2(\xi) \quad (5)$$

where $\bar{G} = \sqrt{|\mathbf{G_1}| \times |\mathbf{G_2}|}$ is the geometric mean of the norms of the gradients of the two PESs and $\mathrm{Ai}(\xi)$ is the Airy function with argument ξ which takes the form

$$\xi = -(\varepsilon_\perp - E_{MECP}) \left(\frac{2\mu_\perp |\Delta\mathbf{G}|^2}{\hbar^2 \bar{G}^4}\right)^{1/3} \quad (6)$$

The WC expression for P_{trans} will then yield non-zero values for energies below E_{MECP}, although it decreases rapidly in this regime, allowing for tunneling from one PES to the other below the crossing point. Note that besides the vibrational analysis of the MECP, the GLOWfreq[51] code also yields $\mu_\perp$, $|\Delta\mathbf{G}|$ and $\bar{G}$, which are necessary quantities for the LZ and WC probability expressions. This information is presented in Table S3 of the ESI.†

In summary, two rate constants were calculated in this work. The LZ rate constant

$$k^{LZ}_{ISC}(T) = \frac{Q_{MECP}(T)}{hQ_R(T)} \int_{E_{MECP}}^\infty P^{LZ}_{trans}(\varepsilon_\perp) \exp(-\beta\varepsilon_\perp) d\varepsilon_\perp \quad (7)$$

which is important for comparison reasons as it operates only in the classically allowed region for energies above the MECP, therefore excluding possible tunneling effects. The other is the more robust WC rate constant

$$k^{WC}_{ISC}(T) = \frac{Q_{MECP}(T)}{hQ_R(T)} \int_0^\infty P^{WC}_{trans}(\varepsilon_\perp) \exp(-\beta\varepsilon_\perp) d\varepsilon_\perp \quad (8)$$

which gathers contributions from both the classically allowed, $E_{MECP} < \varepsilon_\perp < \infty$, and classically forbidden (tunneling) regions, $0 < \varepsilon_\perp < E_{MECP}$.

3 Results and discussion

An overall picture of our results is presented in Fig. 1, where we show the triplet and singlet intrinsic reaction coordinate (IRC) curves originating from the respective saddle-point calculations. Cartesian coordinates and electronic energies for all stationary points are given in the ESI.† Note that each IRC path contemplates a unique concerted motion of atoms and for this reason the reaction coordinate (s) represents, to a greater or lesser extent, different structures for each IRC path. The curves shown in this figure are symmetric with respect to the axis of symmetry given by $s = 0$ which is represented as a black dashed line splitting Fig. 1 into two panels, (a) and (b), where each stationary point in one panel has a corresponding enantiomer in the other

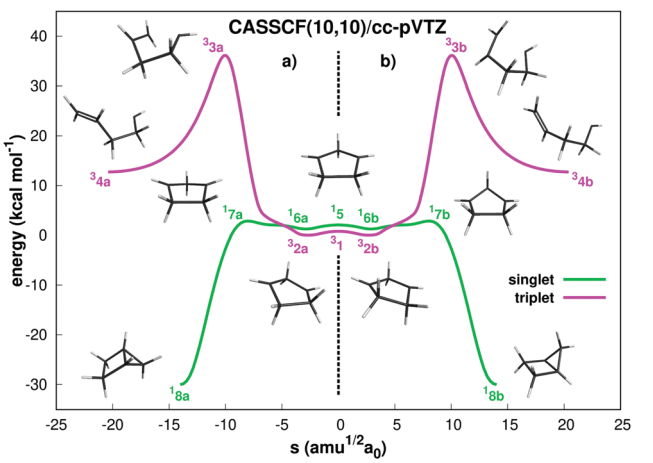

Fig. 1 IRC paths for the triplet (purple) and singlet (green) PESs computed at the CASSCF(10,10)/cc-pVTZ level. The triplet curve includes the cyclopentane-1,3-diyl reactant (^{3}**2**) and the singlet curve includes the bicyclo[2.1.0]pentane product (^{1}**8**). Energies (kcal mol^{-1}) are given relative to ^{3}**2**. The axis of symmetry at $s = 0$ splits the figure into two panels, (a and b). Structures displayed with MacMolPlt.[70]

panel. The stationary points are indicated by a number (along with its associated spin multiplicity) and an "**a**" or a "**b**" (depending on which panel they are located) associating two structures with an enantiomeric pair, all numerically confirmed.[41] The exceptions are the ^{1}**7** and ^{1}**8** stationary points, for which the pair of "**a**" and "**b**" structures are identical, not enantiomers. The reference for zero energy is ^{3}**2**, which represents the enantiomeric pair corresponding to the global minimum of the triplet curve, cyclopentane-1,3-diyl. The active space employed to describe ^{3}**2** consisted of the four σ and four σ* molecular orbitals (MOs) involving the C(3)–C(1)–C(2) bonds of the CH–CH_2–CH fragment and of the two C–H bonds of the sp^3 hybridized central carbon of that fragment. The remaining active orbitals correspond to the two MOs with natural occupation of one resulting from the overlap of the out-of-plane unhybridized p atomic orbitals in the sp^2 hybridized C(3) and C(2) atoms. These ten MOs are shown in the ESI.† The singlet curve leads to bicyclo[2.1.0]pentane, ^{1}**8**, with the ^{1}**7** saddle-points, which separate the ^{1}**6** singlet diradical structures from ^{1}**8**, sharing some resemblance to the structure responsible for the 3.03 kcal mol^{-1} energy barrier reported by others.[31] In addition, although the ^{3}**2** and ^{1}**6** structures occur in pairs, only one structure of each pair was previously accounted for.[31]

Fig. 2 shows a more detailed view of the PESs by zooming in the central region of Fig. 1, where the majority of the stationary points are located. For both curves, the structures with s = 0 correspond to transition states with C_s-like symmetry which link two C_2-like minima, forming double-well potentials.[33] A detailed analysis[41] of the double-well stationary points of the singlet and triplet curves also shows that the sets of structures, (^{3}**2a**,^{1}**6a**), (^{3}**2b**,^{1}**6b**) and (^{3}**1**,^{1}**5**), include identical conformations. For example, the root-mean-square distances[41] (rmsd) between (^{3}**2a**,^{1}**6a**) is 1.6 × 10^{-2} Å while the rmsd between the (^{3}**1**,^{1}**5**) pair of saddle-points is 1.1 × 10^{-2} Å.

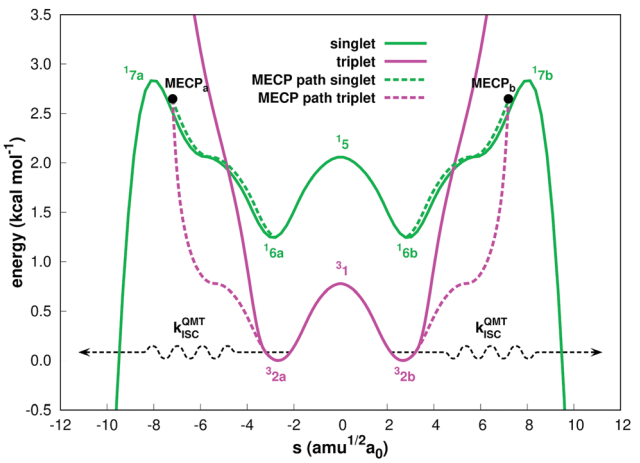

Fig. 2 Zoomed in version of the central region of Fig. 1 but without showing the plot's axis of symmetry at s = 0 and including the pair of MECPs (solid black circles) and their respective steepest descent paths to the minima (purple and green dashed curves). The two dashed black arrows illustrate possible spin-forbidden vibrational ground-state heavy-atom QMT processes.

The singlet–triplet energy gap, E(^{1}**6**)–E(^{3}**2**), was calculated as 1.24 and 1.36 kcal mol^{-1} at the CASSCF(10,10)/cc-pV*T*Z and MC-QDPT(10,10)/cc-pV*T*Z levels, respectively, which is in very close agreement with reported Davidson-corrected TC-CISD calculations.[33] Fig. 2 also clearly shows that when triplet cyclopentane-1,3-diyl is formed (in the ^{3}**2a** and ^{3}**2b** wells) at cryogenic temperatures, the only tunneling possibility within the triplet state will be between the two C_2-like minima, ^{3}**2a** and ^{3}**2b**, since the ^{3}**4** products will not be available at cryogenic temperatures. On the other hand, if one considers tunneling through a spin-forbidden ISC process, the singlet IRC curves become available. Note that when considering an ISC (non-adiabatic process), it is frequently necessary to determine the MECP between the electronic states under consideration, this case between the triplet and the singlet PESs, as it plays a similar role to a transition state in adiabatic reactions.[25,47,49] The two MECPs of C_s-like symmetry were located[48] and identified as identical structures (not enantiomers) at 2.65 kcal mol^{-1} above the ^{3}**2** minima at the CASSCF(10,10)/cc-pV*T*Z level of theory, without inclusion of zero-point energy (ZPE), see Fig. 2. The dashed lines represent the steepest descent path from the MECPs to the ^{3}**2** and ^{1}**6** minima and were obtained with the Gonzalez–Schlegel method,[71] which was also used to calculate the singlet and triplet IRC curves. No other low-energy MECPs were found connecting these minima. The structures of the MECPs are very similar to the ^{1}**7** saddle-points, with an rmsd of only 7.6 × 10^{-2} Å between them. To the best of our knowledge, this is the first time that MECPs are being reported for this reaction. Based on the computed PESs, it becomes evident that the ring-closure of triplet cyclopentane-1,3-diyl to singlet bicyclo[2.1.0]pentane at cryogenic temperatures can only take place through a spin-forbidden heavy-atom QMT mechanism promoted by SOC in the region of the located MECPs. The SOC, which is fundamental in ISC since it is responsible for mixing electronic states of different spins,[53] was estimated to be 0.34 cm^{-1}, in line with recent suggestions of a low value,[31] which is normally indicative of low probabilities of transition between spin-diabatic states.

As far as we know, within the specific framework of calculating spin-forbidden vibrational ground-state heavy-atom QMT rate constants, the WC formulation of NA-TST was used only once,[16] with the calculations showing a very good agreement (albeit potentially accidental[25,54] in a similar fashion as observed in canonical TST) to the already discussed experimental results of reactions shown in Scheme 1a and b.[14,16] We performed our calculations in the temperature range of 5 to 500 K. At 5 and 20 K, the temperatures used in the most recent experiments in argon matrices,[31] tunneling accounts for 100% of the rate constant value. In conventional TST it is usual for the rate expression to include a reaction-path symmetry number[72] σ (not to confuse with the molecular orbital symbol) given by the ratio between the rotational symmetry numbers of the reactant (R) and transition state (TS), $\sigma = \sigma_{rot,R}/\sigma_{rot,TS}$. Since in this work we are dealing with an enantiomeric reactant pair and, in practice, with only one MECP, we can utilize the same approach and adapt eqn (16) of ref.

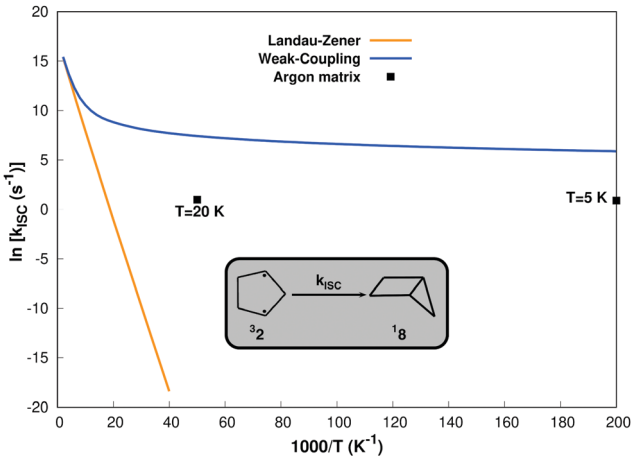

Fig. 3 Arrhenius plots of the LZ (orange, does not include tunneling) and WC (blue, includes tunneling) gas-phase NA-TST rate constants. Two data points, corresponding to experimental observations in argon matrices, are also included.

72 as

$$\sigma = \frac{\sigma_{\mathrm{rot},^3\mathbf{2}}}{2\sigma_{\mathrm{rot,MECP}}} \quad (9)$$

Introducing the values (Table 2 of ref. 72) for the rotational symmetry numbers corresponding to the C_2 ($\sigma_{\mathrm{rot},^3\mathbf{2}} = 2$) and C_s ($\sigma_{\mathrm{rot,MECP}} = 1$) symmetry point groups in the previous equation gives $\sigma = 1$. The Arrhenius plots of the LZ and WC gas-phase rate constants are shown in Fig. 3 (data from Table S4 in the ESI†), with the WC curve showing a typical tunneling behaviour. The WC rate constants at 5 and 20 K were calculated as 356 and 1670 s^{-1}, respectively, in a reasonable agreement with the corresponding experimental rate constants[31] in argon matrices of 2.48 and 2.71 s^{-1}. This overestimation deserves a comment. Besides the approximations inherited from being a statistical theory closely related to TST[25] and other issues related to the Airy approximation in the low-energy regime,[68,73–75] the WC formulation of NA-TST does not take into account the curvature of the crossing diabatic PESs, simply assuming a linear crossing with the slopes calculated by the energy gradients at the MECP. The width of the resulting triangular barrier will often be too narrow compared to the true crossing barrier,[54,74] thus overestimating the tunneling probability and the respective rate constant. This certainly seems to be the case here, since our sloped intersection connects the MECP to the $^1\mathbf{6}$ minima instead of the bicyclo[2.1.0]pentane product directly. However, this overestimation does not alter the fundamental qualitative trends of this reaction. A minimal temperature dependence is observed for low temperatures in the WC curve, with the tunneling region being responsible for the totality of the rate constant value up to 50 K, thus reinforcing the compelling evidence for a spin-forbidden heavy-atom QMT reaction at cryogenic temperatures.

4 Conclusions

Our theoretical studies solved a long-standing problem by unequivocally showing that, at cryogenic temperatures, the ring closure of triplet cyclopentane-1,3-diyl to singlet bicyclo[2.1.0]pentane occurs through spin-forbidden heavy-atom (carbon) QMT. To reach this conclusion, a description of the singlet and triplet PESs was performed with *ab initio* multireference electronic structure calculations, which included, as far as we know, the first report of MECPs between the singlet and triplet PESs. Additionally, we performed rate constant calculations for the reaction of triplet ground-state cyclopentane-1,3-diyl with the WC formulation of NA-TST, therefore accounting for the spin-forbidden nature of the problem while also including QMT effects. Despite the limitations of this formulation, the calculations predict a tunneling regime occurring spontaneously at low temperature in fair agreement with experimental observations, thus providing solid evidence confirming the 45-year-old hypothesis that the title reaction is driven by spin-forbidden heavy-atom QMT. Besides solving a fundamental problem, this study shows that, despite its simplicity and limitations, the WC formulation of NA-TST can be used to explore and unlock a deeper understanding of chemical reactivity involving spin-forbidden reactions in the low temperature regime.

Conflicts of interest

There are no conflicts to declare.

Acknowledgements

This work was supported by Project POCI-01-0145-FEDER-028973, funded by FEDER, *via* Portugal 2020-POCI, and by National Funds *via* the Portuguese Foundation for Science and Technology (FCT). The Coimbra Chemistry Centre is supported by the FCT through the projects UIDB/00313/2020 and UIDP/00313/2020, co-funded by COMPETE. L. P. V. acknowledges the Coimbra Chemistry Centre for the CQC-SER-C2-BPD research grant. C. M. N. acknowledges the FCT for an Auxiliary Researcher grant.

Notes and references

1 E. Merzbacher, *Phys. Today*, 2002, **55**, 44–49.
2 R. P. Bell, *Proc. R. Soc. London, Ser. A*, 1933, **139**, 466–474.
3 R. P. Bell, *Proc. R. Soc. London, Ser. A*, 1935, **148**, 241–250.
4 A. M. Orendt, B. R. Arnold, J. G. Radziszewski, J. C. Facelli, K. D. Malsch, H. Strub, D. M. Grant and J. Michl, *J. Am. Chem. Soc.*, 1988, **110**, 2648–2650.
5 P. S. Zuev and R. S. Sheridan, *J. Am. Chem. Soc.*, 1994, **116**, 4123–4124.
6 P. S. Zuev, R. S. Sheridan, T. V. Albu, D. G. Truhlar, D. A. Hrovat and W. T. Borden, *Science*, 2003, **299**, 867–870.
7 R. A. Moss, R. R. Sauers, R. S. Sheridan, J. Tian and P. S. Zuev, *J. Am. Chem. Soc.*, 2004, **126**, 10196–10197.
8 H. Inui, K. Sawada, S. Oishi, K. Ushida and R. J. McMahon, *J. Am. Chem. Soc.*, 2013, **135**, 10246–10249.

9 M. Ertelt, D. A. Hrovat, W. T. Borden and W. Sander, *Chem. – Eur. J.*, 2014, **20**, 4713–4720.
10 C. M. Nunes, I. Reva, S. Kozuch, R. J. McMahon and R. Fausto, *J. Am. Chem. Soc.*, 2017, **139**, 17649–17659.
11 T. Schleif, J. Mieres-Perez, S. Henkel, M. Ertelt, W. T. Borden and W. Sander, *Angew. Chem., Int. Ed.*, 2017, **56**, 10746–10749.
12 T. Schleif, J. Mieres-Perez, S. Henkel, E. Mendez-Vega, H. Inui, R. J. McMahon and W. Sander, *J. Org. Chem.*, 2019, **89**, 16013–16018.
13 T. Schleif, J. Tatchen, J. F. Rowen, F. Beyer, E. Sanchez-Garcia and W. Sander, *Chem. – Eur. J.*, 2020, **26**, 10452–10458.
14 Z. Wu, R. Feng, H. Li, J. Xu, G. Deng, M. Abe, D. Bégué, K. Liu and X. Zeng, *Angew. Chem., Int. Ed.*, 2017, **56**, 15672–15676.
15 C. M. Nunes, A. K. Eckhardt, I. Reva, R. Fausto and P. R. Schreiner, *J. Am. Chem. Soc.*, 2019, **141**, 14340–14348.
16 C. M. Nunes, L. P. Viegas, S. A. Wood, J. P. L. Roque, R. J. McMahon and R. Fausto, *Angew. Chem., Int. Ed.*, 2020, **59**, 17622–17627.
17 P. R. Schreiner, *J. Am. Chem. Soc.*, 2017, **139**, 15276–15283.
18 D. Ley, D. Gerbig and P. R. Schreiner, *Org. Biomol. Chem.*, 2012, **10**, 3781–3790.
19 S. Karmakar and A. Datta, *J. Phys. Chem. B*, 2016, **120**, 945–950.
20 A. Nandi, D. Gerbig, P. R. Schreiner, W. T. Borden and S. Kozuch, *J. Am. Chem. Soc.*, 2017, **139**, 9097–9099.
21 C. Doubleday, R. Armas, D. Walker, C. V. Cosgriff and E. M. Greer, *Angew. Chem., Int. Ed.*, 2017, **56**, 13099–13102.
22 X. Li, T. Liao and L. W. Chung, *J. Am. Chem. Soc.*, 2017, **139**, 16438–16441.
23 C. S. Michel, P. P. Lampkin, J. Z. Shezaf, J. F. Moll, C. Castro and W. L. Karney, *J. Am. Chem. Soc.*, 2019, **141**, 5286–5293.
24 C. Castro and W. L. Karney, *Angew. Chem., Int. Ed.*, 2020, **59**, 8355–8366.
25 J. N. Harvey, *Wiley Interdiscip. Rev.: Comput. Mol. Sci.*, 2014, **4**, 1–14.
26 C. M. Nunes, S. N. Knezz, I. Reva, R. Fausto and R. J. McMahon, *J. Am. Chem. Soc.*, 2016, **138**, 15287–15290.
27 MarvinSketch was used for drawing and displaying chemical structures, MarvinSketch 20.21.0, ChemAxon (https://www.chemaxon.com).
28 S. L. Buchwalter and G. L. Closs, *J. Am. Chem. Soc.*, 1975, **97**, 3857–3858.
29 M. B. Sponsler, R. Jain, F. D. Coms and D. A. Dougherty, *J. Am. Chem. Soc.*, 1989, **111**, 2240–2252.
30 W. T. Borden, *Wiley Interdiscip. Rev.: Comput. Mol. Sci.*, 2016, **6**, 20–46.
31 S. K. Sarkar, E. Solel, S. Kozuch and M. Abe, *J. Org. Chem.*, 2020, **85**, 8881–8892.
32 M. Abe, *Chem. Rev.*, 2013, **113**, 7011–7088.
33 C. D. Sherrill, E. T. Seidl and H. F. Schaefer III, *J. Phys. Chem.*, 1992, **96**, 3712–3716.
34 B. K. Carpenter, *Org. Biomol. Chem.*, 2004, **2**, 103–109.
35 P. Siegbahn, A. Heiberg, B. Roos and B. Levy, *Phys. Scr.*, 1980, **21**, 323–327.
36 B. O. Roos, P. R. Taylor and P. E. M. Siegbahn, *Chem. Phys.*, 1980, **48**, 157–173.
37 P. E. M. Siegbahn, J. Almlöf, A. Heiberg and B. O. Roos, *J. Chem. Phys.*, 1981, **74**, 2384–2396.
38 K. Ruedenberg, M. W. Schmidt, M. M. Gilbert and S. T. Elbert, *Chem. Phys.*, 1982, **71**, 41–49.
39 T. H. Dunning, *J. Chem. Phys.*, 1989, **90**, 1007–1023.
40 M. W. Schmidt, K. K. Baldridge, J. A. Boatz, S. T. Elbert, M. S. Gordon, J. H. Jensen, S. Koseki, N. Matsunaga, K. A. Nguyen, S. Su, T. L. Windus, M. Dupuis and J. A. Montgomery, Jr., *J. Comput. Chem.*, 1993, **14**, 1347–1363.
41 J. M. C. Marques, J. L. Llanio-Trujillo, P. E. Abreu and F. B. Pereira, *J. Chem. Inf. Model.*, 2010, **50**, 2129–2140.
42 H. Nakano, *J. Chem. Phys.*, 1993, **99**, 7983–7992.
43 H. Nakano, *Chem. Phys. Lett.*, 1993, **207**, 372–378.
44 J. N. Harvey and M. Aschi, *Phys. Chem. Chem. Phys.*, 1999, **1**, 5555–5563.
45 J. N. Harvey and M. Aschi, *Faraday Discuss.*, 2003, **124**, 129–143.
46 J. N. Harvey, R. Poli and K. M. Smith, *Coord. Chem. Rev.*, 2013, **238–239**, 347–361.
47 J. N. Harvey, *Phys. Chem. Chem. Phys.*, 2007, **9**, 331–343.
48 A. Farazdel and M. Dupuis, *J. Comput. Chem.*, 1991, **12**, 276–282.
49 J. N. Harvey, M. Aschi, H. Schwarz and W. Koch, *Theor. Chem. Acc.*, 1998, **99**, 95–99.
50 W. H. Miller, N. C. Handy and J. E. Adams, *J. Chem. Phys.*, 1980, **72**, 99–112.
51 K. L. Gannon, M. A. Blitz, C.-H. Liang, M. J. Pilling, P. W. Seakins, D. R. Glowacki and J. N. Harvey, *Faraday Discuss.*, 2010, **147**, 173–188.
52 D. G. Fedorov, S. Koseki, M. W. Schmidt and M. S. Gordon, *Int. Rev. Phys. Chem.*, 2003, **22**, 551–592.
53 C. M. Marian, *Wiley Interdiscip. Rev.: Comput. Mol. Sci.*, 2012, **2**, 187–203.
54 A. O. Lykhin and S. A. Varganov, *Phys. Chem. Chem. Phys.*, 2020, **22**, 5500–5508.
55 B. H. Lengsfield, J. A. Jafri, D. H. Phillips and C. W. Bauschlicher, *J. Chem. Phys.*, 1981, **74**, 6849–6856.
56 A. O. Lykhin, D. S. Kaliakin, G. E. dePolo, A. A. Kuzubov and S. A. Varganov, *Int. J. Quantum Chem.*, 2016, **116**, 750–761.
57 J. B. Delos, *J. Chem. Phys.*, 1973, **59**, 2365–2369.
58 J. C. Tully, *J. Chem. Phys.*, 1974, **61**, 61–68.
59 G. E. Zahr, R. K. Preston and W. H. Miller, *J. Chem. Phys.*, 1975, **62**, 1127–1135.
60 E. J. Heller and R. C. Brown, *J. Chem. Phys.*, 1983, **79**, 3336–3351.
61 J. C. Lorquet and B. Leyh-Nihant, *J. Phys. Chem.*, 1988, **92**, 4778–4783.
62 Q. Cui, K. Morokuma, J. M. Bowman and S. J. Klippenstein, *J. Chem. Phys.*, 1999, **110**, 9469–9482.
63 S. Liu, S. Srinivasan, J. Tao, M. C. Grady, M. Soroush and A. M. Rappe, *J. Phys. Chem. A*, 2014, **118**, 9310–9318.
64 W. Forst, *Unimolecular Reactions: A Concise Introduction*, Cambridge University Press, Cambridge, 2003.
65 L. D. Landau, *Phys. Z. Sowjetunion*, 1932, **2**, 46–51.

66 C. Zener, *Proc. R. Soc. London, Ser. A*, 1932, **137**, 696–702.
67 J. C. Tuly, *J. Chem. Phys.*, 2012, **137**, 22A301.
68 L. D. Landau and E. M. Lifshitz, *Quantum Mechanics. Non-relativistic Theory*, Pergamon Press Ltd., Oxford, England, 2nd (revised) edn, 1965.
69 P. V. Coveney, M. S. Child and A. Bárány, *J. Phys. B: At. Mol. Phys.*, 1985, **18**, 4557–4580.
70 B. M. Bode and M. S. Gordon, *J. Mol. Graphics Modell.*, 1998, **16**, 133–138.
71 C. Gonzalez and H. B. Schlegel, *J. Chem. Phys.*, 1989, **90**, 2154–2161.
72 A. Fernández-Ramos, B. A. Ellingson, R. Meana-Pañeda, J. M. C. Marques and D. G. Truhlar, *Theor. Chem. Acc.*, 2007, **118**, 813–826.
73 E. E. Nikitin and S. Y. Umanskii, *Theory of Slow Atomic Collisions*, Springer-Verlag, Berlin, Heidelberg, 1984, ch. The Linear Two-State Landau-Zener Model, vol. 30, pp. 273–312.
74 E. I. Dashevskaya, E. E. Nikitin and J. Troe, *Phys. Chem. Chem. Phys.*, 2015, **17**, 151–158.
75 E. I. Dashevskaya, E. E. Nikitin and H.-J. Troe, *Z. Phys. Chem.*, 2018, **232**, 311–323.